Chemical Engineering Journal 538 (2026) 176570

Contents lists available at ScienceDirect

Chemical Engineering Journal

journal homepage: www.elsevier.com/locate/cej

High-thermopower ionic thermoelectric hydrogel with gradient immobilization of anions by polypyrrole

Zhou Li [a,1], Wenzhuo Zhao [a,1], Shouze Li [a], Dongyan Xu [b], Wonjoon Choi [c,*], Run Hu [a,d,**]

[a] School of Energy and Power Engineering, Huazhong University of Science and Technology, Wuhan, 430074, China
[b] Department of Mechanical and Automation Engineering, The Chinese University of Hong Kong, Shatin, New Territories, Hong Kong Special Administrative Region
[c] School of Mechanical Engineering, Korea University, Seoul, 02841, Republic of Korea
[d] Department of Applied Physics, Kyung Hee University, 1732 Deogyeong-daero, Giheung-gu, Yongin-Si, Gyeonggi-do, 17104, Republic of Korea

ARTICLE INFO

Keywords:
Gradient immobilization
Ionic thermoelectrics
Thermodiffusion

ABSTRACT

Ionic thermoelectric (i-TE) materials, which convert heat into electricity via the Soret effect, have attracted considerable interest due to their high thermopower and excellent flexibility. Restricting the thermal diffusion of either cations or anions has been demonstrated as an effective strategy to enhance thermoelectric performance; however, existing studies remain largely limited to systems with uniform concentration distributions. In this work, we develop a P-type thermoelectric hydrogel, denoted as PVA/PPy/GF@5.00%SDBS, which achieves a giant Seebeck coefficient of 21.5 $mV{\cdot}K^{-1}$, representing 2.5-fold and 7-fold enhancements over uniformly immobilized and pristine systems, respectively. This exceptional performance is enabled by a gradient immobilization strategy that restricts anion diffusion while simultaneously increasing the Eastman entropy associated with cation transport. Collectively, these findings elucidate the role of ion immobilization in modulating the Soret effect and establish a new paradigm for controlling ion migration in i-TE systems.

1. Introduction

More than half of the energy generated from human production and daily activities is discharged to the environment as waste heat, a significant portion of which exists as low-grade thermal energy with temperature differences of only tens of degrees or even just a few degrees above ambient conditions [1–4]. Harnessing and utilizing such low-grade thermal energy is crucial for mitigating global warming and addressing environmental changes. Ionic thermoelectric (i-TE) materials enable direct conversion between thermal energy (human body heat, low-grade heat, industrial waste heat, etc.) and electric energy through the ionic Soret effect [5]. The Soret effect, also known as the thermodiffusion effect, refers to the phenomenon where ions form a concentration gradient under a temperature gradient. The thermal diffusion capability of ions is positively correlated with their Eastman entropy S^*. Due to the difference in thermal diffusion coefficients between anions and cations, the overall electrical neutrality of the electrolyte is disrupted. This discrepancy leads to the formation of distinct charge distributions at the hot and cold electrodes, as illustrated in **Fig. 1**(a), and consequently induces polarization of the electric double layer. When an external load is connected across the electrodes at this point, the system discharges, generating an electric current in the circuit and gradually restoring electrical neutrality within the electrolyte. The thermodiffusion effect delivers electrical energy in a capacitive manner, as there is no direct electron exchange between the electrolyte and the electrodes. Therefore, a certain amount of time is required after each discharge to prepare for the subsequent discharge process.

Based on the Onsager transport theory, the conversion of heat into electricity can be described by the Seebeck coefficient (Se), also known as thermopower, which is defined as

$$Se = -\frac{\Delta E}{\Delta T} = \frac{\sum q_i n_i S_i^* D_i}{\sum q_i^2 n_i D_i} \quad (1)$$

where q, n, and D represent the quantity of electricity, ion concentration, and diffusion coefficient, respectively, and the subscript i denotes the ion species. In ionic thermoelectric systems, a positive Seebeck coefficient ($Se > 0$) indicates that the thermodiffusion is dominated by

* Corresponding author.
** Correspondence to: R. Hu, School of Energy and Power Engineering, Huazhong University of Science and Technology, Wuhan, 430074, China.
E-mail addresses: wojchoi@korea.ac.kr (W. Choi), hurun@hust.edu.cn (R. Hu).
[1] These authors contributed equally to this work.

https://doi.org/10.1016/j.cej.2026.176570
Received 14 January 2026; Received in revised form 27 March 2026; Accepted 21 April 2026
Available online 22 April 2026

cations, which is referred to as P-type ionic thermoelectric behavior in this work.

In comparison with semiconductor thermoelectric materials, ionic thermoelectric materials exhibit several distinct advantages, such as high thermopower, flexibility, and cost-effectiveness, which have attracted extensive research interest [6–9]. However, the low energy density of low-grade thermal energy poses considerable challenges for its conversion into usable electrical power (~V). Therefore, enhancing the thermopower and figure of merit (*ZT*) of i-TE materials is crucial for practical applications [9–12]. To improve the energy conversion efficiency and minimize the integrated system volume, research efforts have increasingly focused on increasing the thermopower of i-TE systems [13–16]. A variety of strategies have been reported to enhance the thermopower of i-TE materials, including gelator engineering [17], additive engineering [18–20], antisolvent engineering [21], ionic doping [1,22–26], interfacial engineering [27,28], and phase transition [29]. Furthermore, i-TE materials with additional functionalities, such as stretchability [30,31], and self-healing capability [32–34], have also been developed recently. These approaches generally aim to constrain the thermally induced migration of either anions or cations in homogeneous systems, thereby amplifying the disparity in thermodiffusion behavior. Most of these studies rely on easily fabricated homogeneous systems, where the constrained ions are uniformly distributed at a fixed concentration. Nevertheless, a fundamental question remains largely unexplored: does a non-uniform distribution of constrained ions have an impact on thermoelectric performance?

In this work, we propose a novel strategy for enhancing the thermopower of ionic thermoelectric materials through gradient immobilization of anions. In the designed system, anions are immobilized within the polypyrrole (PPy) backbone due to their large size, while cations are free to migrate throughout the structure. We validate the feasibility and effectiveness of this approach using both electrochemical theory and experimental measurements. It is demonstrated that when the immobilized anions exhibit a concentration gradient increasing from the cold end to the hot end, the thermopower is significantly enhanced. Conversely, a reverse gradient leads to its suppression. The optimized ionic thermoelectric system achieves a high thermopower of 21.5 $mV \cdot K^{-1}$ and a *ZT* value of 0.645. This study introduces the concept of concentration gradient into the design of ionic thermoelectric capacitors, offering new insights and methodologies for advancing the performance of i-TE systems.

2. Experimental section

2.1. Materials

PVA-117 (≥99%, Aladdin Reagent), sodium dodecyl benzene sulfonate (SDBS, ≥95%, Sarn Chemical Technology), ammonium persulfate

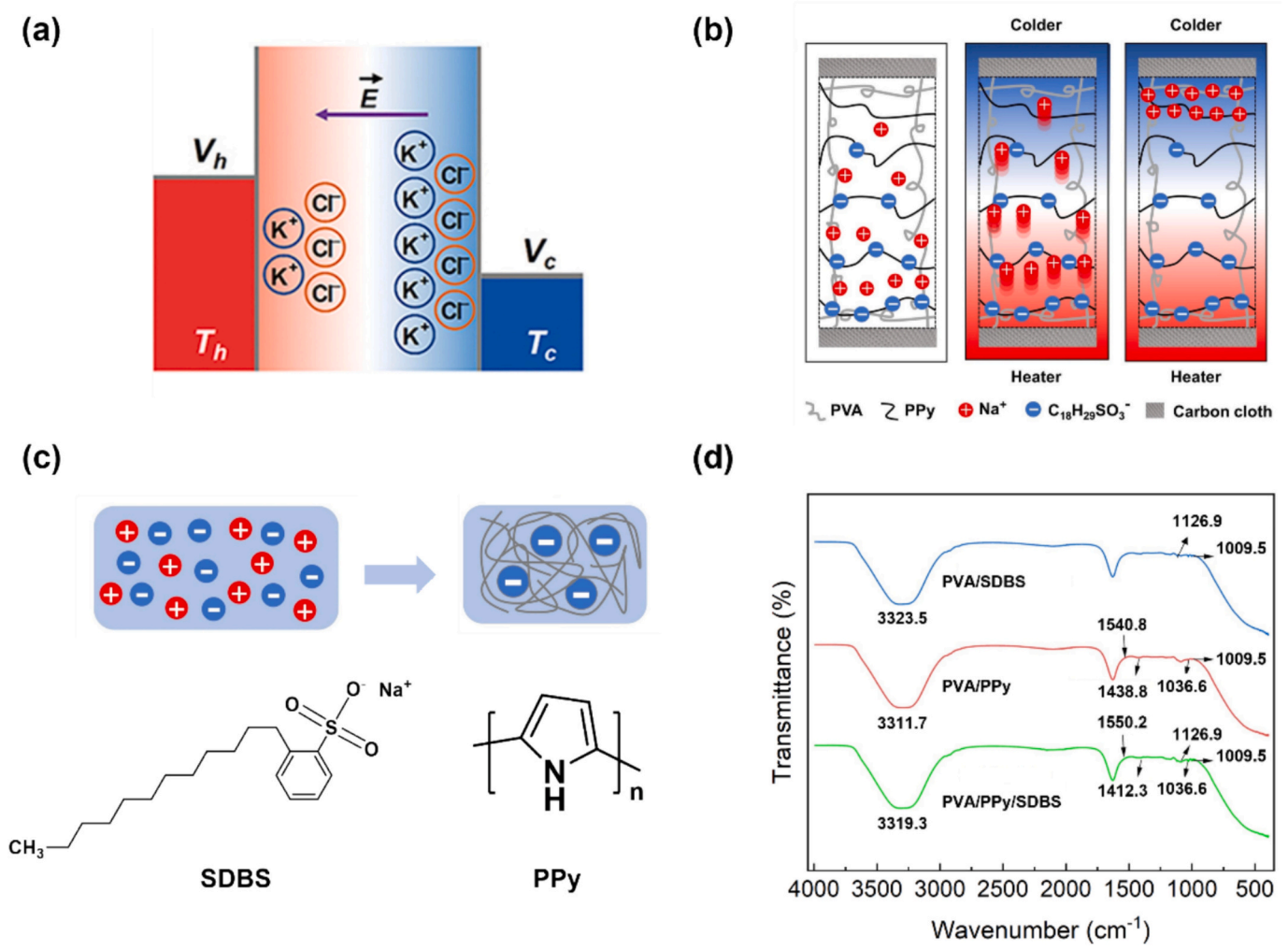

Fig. 1. Schematic illustrations, molecular structure, and characterization of the ionic thermoelectric hydrogel. (a) Thermaldiffusion effect in ionic systems. (b) Proposed ion transport mechanism under a thermal gradient in the PVA/PPy/GF hydrogel with gradient-immobilized anions. (c) Schematic illustration of PPy doped with large anions, along with the molecular structures of SDBS and PPy. (d) FTIR spectra of the PVA/SDBS, PVA/PPy, and PVA/PPy/SDBS hydrogels.

(APS, ≥98%, Sinopharm Chemical Reagent), and pyrrole (C_4H_5N, ≥99%, Sarn Chemical Technology). Deionized water (18.2 MΩ·cm) was used throughout all experiments. All chemicals were used as received without further purification.

2.2. Preparation of ionic thermoelectric hydrogels

The preparation procedure for PVA-based hydrogels is schematically illustrated in Fig. S2. First, 3.0 g PVA was dissolved in 30 mL deionized water under continuous stirring at 95 °C for 60 min to form a well-dispersed solution. Then, 6 mL of pyrrole was added to the PVA solution and stirred for another 10 min. The resulting mixture was degassed under vacuum for 5 min. The solution was then cast into custom molds and frozen at −20 °C for 24 h, followed by thawing at room temperature for 3 h. This freeze–thaw cycle was repeated three times to form a physically crosslinked PVA hydrogel. To prepare the PVA@SDBS hydrogel, the as-prepared PVA hydrogel was immersed in SDBS solutions of different mass fractions (2.50%, 3.75%, 5.00%, 6.75%, 7.50%) for 3 h. For the PVA/PPy/UF hydrogel, the pristine PVA hydrogel was immersed for 3 h in the same series of SDBS solutions containing ammonium persulfate. This allowed SDBS to uniformly diffuse into the hydrogel network, while ammonium persulfate initiated the polymerization of pyrrole, leading to the homogeneous immobilization of anions within the PPy backbone. For the PVA/PPy/GF hydrogel, a gradient distribution of anions was achieved by dropwise addition of SDBS solution containing ammonium persulfate onto the pristine PVA hydrogel over 3 h. Due to the sequential absorption across the hydrogel thickness, a spatial gradient in SDBS concentration was established, resulting in gradient immobilization of anions in the PPy backbone. Unless otherwise specified, all thermoelectric measurements were conducted at 298 K under ambient relative humidity (50–70%). All samples were tested under identical environmental conditions to ensure reliable comparison. It should be noted that the water content in hydrogels may influence ionic transport; however, the comparative trends reported in this work remain valid under consistent testing conditions.

2.3. Thermoelectric measurements

The ionic Seebeck coefficient was measured using a well-designed experimental setup shown in Fig. S3. The system comprises two Peltier cooling devices mounted on a PTFE base plate, with carbon cloth electrodes attached to the substrate. The temperatures at the hot and cold ends of the sample (T_H and T_C) were monitored using two T-type thermocouples affixed to the carbon cloth electrode. The hydrogel samples were cut into rectangular specimens measuring 15 mm × 30 mm × 4 mm. A Keithley 2700 in the open circuit mode was used to monitor the electrical signal between the two wires. The temperature difference across the sample could be controlled by tuning the current applied to the Peltier modules. The Seebeck coefficient was extracted after the thermovoltage reached a steady state, defined as a stable plateau where the voltage variation with time became negligible within the measurement duration. The Seebeck coefficient was calculated using Eq. (1), where ΔE represents the open circuit voltage, ΔT denotes the temperature difference measured by the T-type thermocouples. The hydrogel samples were positioned such that the temperature gradient was applied across the thickness direction, which is consistent with the direction of the anion concentration gradient. Carbon cloth electrodes were attached to the two opposite faces corresponding to the hot and cold sides, ensuring that the ion transport direction is aligned with both the temperature gradient and the gradient distribution of immobilized anions.

2.4. Electrochemical measurements

For cyclic voltammetry (CV) measurements, the hydrogels were placed in a cylindrical container and scanned within a voltage window of −0.4 V to +0.4 V using a DH 7001 A electrochemical workstation. A Pt electrode was employed as the working electrode, while a graphite electrode served as both the counter and reference electrode. Scan rates of 10, 20, 50, and 100 mV•s^{-1} were applied. Electrochemical impedance spectroscopy (EIS) was conducted using the same DH 7001 A electrochemical workstation. The hydrogels were filled in a cylindrical container and tested under open-circuit conditions with an AC voltage amplitude of 10 mV over a frequency range of 0.1 Hz to 100 kHz. The minimum value in the Nyquist diagram of the negative imaginary part of the impedance relative to the real part is used as the sampling resistance. The ionic conductivity σ was then calculated according to Eq. (2),

$$\sigma = \frac{l}{RA} \tag{2}$$

where l denotes the distance between the electrodes, R represents the measured resistance, and A is the contact area between the electrode and the hydrogel.

2.5. Thermal conductivity measurement and Fourier transform

The hydrogel was cut into specimens measuring 60 × 40 × 4 mm^3 for thermal conductivity characterization. Thermal conductivity was measured using a hot-wire method (TC3000, China). During testing, the thermal sensor was placed between two identical hydrogel pieces, and the logarithmic relationship between temperature rise and time was recorded. Each sample was measured three times, and the average value was reported. Fourier transform infrared (FTIR) spectra of PVA/SDBS, PVA/PPy, and PVA/PPy/SDBS hydrogel were recorded on an FTIR spectrometer (Nicolet iS50R).

3. Results and discussion

3.1. Regulation of ion transport

PPy is a typical conductive polymer characterized by a large conjugated double bond structure. However, pristine PPy often exhibits suboptimal conductivity and adsorption properties. To address this issue, doping is commonly employed. When PPy is doped with small-sized anions, these anions can readily exchange with those in the solution. Conversely, when large-sized anions are used as dopants, they become immobilized within the PPy backbone, as illustrated in Fig. 1(c).

In this study, SDBS was introduced as a dopant into the PVA/PPy matrix, leading to the effective immobilization of anions within the PPy backbone, as depicted in Fig. 1(b). Under a temperature gradient, the Soret effect typically drives cationic and anionic species to diffuse in opposite directions. However, due to the effectively immobilization of SDBS anions within the PPy backbone, their migration is effectively restricted. This leads to a significant potential difference between the cold and hot junctions due to the differing charge distributions. Fig. 1(d) shows the FTIR spectra of PVA/SDBS, PVA/PPy, and PVA/PPy/SDBS hydrogels. The FTIR spectrum of PVA/SDBS exhibits a characteristic peak at 1126.9 cm^{-1}, assigned to the S—O stretching. The FTIR spectrum of PVA/PPy exhibits several distinctive bands corresponding to the C—H in-plane deformation vibration at 1036.6 cm^{-1}, C—C asymmetric stretching vibration at 1438.8 cm^{-1}, and the ring-stretching mode of the pyrrole ring at 1540.8 cm^{-1} [25]. Notably, in the PVA/PPy/SDBS spectrum, the pyrrole ring-stretching vibration shifts from 1540.8 cm^{-1} to 1550.2 cm^{-1}. This blue shift confirms a molecular-level interaction between PPy and dodecylbenzenesulfonic acid, evidencing effectively doping and ionic immobilization.

3.2. Thermoelectric performance

The thermovoltage response of the PVA/PPy/GF@5.00%SDBS hydrogel exhibits a pronounced dependence on temperature, as shown

in Fig. 2(a). Corresponding thermovoltage curves for other mass fractions are presented in Fig. S4. As depicted in Fig. 2(b), the thermoelectric potential varies linearly with temperature difference across the measured range. To evaluate the effect of anion immobilization on thermoelectric performance, the thermoelectric potential of PVA@SDBS and PVA/PPy/UF hydrogel was compared, as shown in Fig. 2(c). These comparative systems, including PVA@SDBS, PVA/PPy/UF, and PVA/PPy/GF, allow us to systematically distinguish the individual contributions of SDBS incorporation, as well as the effects of uniform versus gradient anion immobilization induced by PPy. The results indicate that the Seebeck coefficient of the hydrogel increases by nearly three times after anion immobilization. According to electrochemical theory, $Se \propto (\alpha_+ - \alpha_-)$ in the PVA@SDBS hydrogel, whereas $Se \propto \alpha_+$ in the PVA/PPy/UF system. The restricted diffusion of anions in the latter system limits electrode polarization primarily to cation migration, leading to a higher Seebeck coefficient in the PVA/PPy/UF hydrogel compared to PVA@SDBS.

Additionally, as the SDBS concentration increases from 2.50% to 7.50%, the number of freely moving cations rises correspondingly, leading to a maximum *Se* of 8.94 $mV \cdot K^{-1}$ at 5.00% concentration. However, a further increase to 7.50% leads to a decline in *Se* to 7.33 $mV \cdot K^{-1}$. This reduction can be attributed to diminished ion selectivity caused by the compression of the Debye length within the polymer matrix. The elevated ion concentration induces a screening effect that compromises the capacity of polymer to selectively facilitate ion migration, thus reducing ion selectivity—a phenomenon consistent with previous reports.

In contrast to the uniform anion distribution in PVA/PPy/UF hydrogels, the PVA/PPy/GF hydrogels exhibit a gradient distribution of anions. According to thermodiffusion theory (Supporting Note 1), the Seebeck coefficient is enhanced when the concentration of immobilized anions is higher at the hot end than at the cold end. As shown in Fig. 2 (c), the thermoelectric properties of PVA/PPy/GF hydrogels with SDBS mass fractions ranging from 2.50% to 7.50% were systematically measured and compared with those of the PVA/PPy/UF counterparts. It should be noted that such a spatially non-uniform distribution introduces an additional electrochemical potential gradient under a temperature bias. Specifically, when the concentration of immobilized anions increases toward the hot side, the resulting asymmetry in ion distribution enhances the thermodiffusion imbalance between cations and anions. Because the mobility of anions is significantly restricted, the thermoelectric response becomes dominated by cation migration, while the gradient term further amplifies the electrochemical potential difference between the two electrodes. Therefore, the PVA/PPy/GF hydrogels develop a more pronounced ion concentration difference between the hot and cold ends under a temperature gradient, resulting in a significant enhancement in thermopower, which is consistent with the theoretical analysis presented in Supporting Note 1. Notably, the thermopower is increased by nearly 2.5 times compared with the uniformly immobilized system.

To further verify the spatial distribution of SDBS, the sulfur content in PVA/PPy/UF and PVA/PPy/GF hydrogels (5.00% SDBS) was quantified using the combustion method. Since sulfur originates exclusively from SDBS, its distribution directly reflects that of the dopant. As shown in Fig. 2(d), the sulfur mass fraction remains uniform in PVA/PPy/UF hydrogels but exhibits a clear gradient in PVA/PPy/GF hydrogels, confirming the successful construction of the gradient anion distribution.

Although Na^+ is employed as a representative cation in this study, it is recognized that cation-dependent factors, such as hydration entropy and ion–polymer interactions, may influence thermoelectric performance. Extending this gradient immobilization strategy to other cation systems will be an important direction for future investigation.

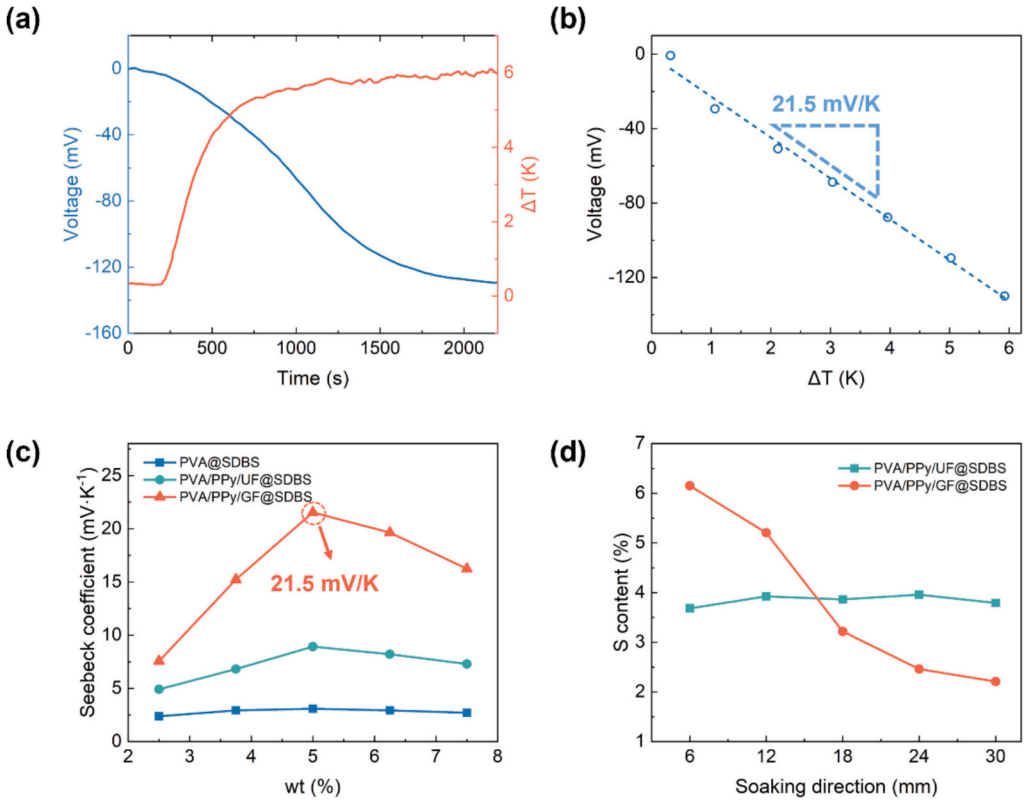

Fig. 2. Thermoelectric performance and compositional analysis of the hydrogels. (a) Thermally induced voltage response of the PVA/PPy/GF@5.00%SDBS hydrogel under a temperature gradient of ~6 K. (b) The corresponding Seebeck coefficient determined by the linear fit of the open-circuit voltage versus temperature difference. (c) Comparison of Seebeck coefficients for PVA@SDBS, PVA/PPy/UF, and PVA/PPy/GF hydrogels as a function of SDBS mass fraction. (d) Spatial distribution of sulfur content in PVA/PPy/UF and PVA/PPy/GF hydrogels.

3.3. Material characterization of PVA@SDBS gel

The typical cyclic voltammetry (CV) characteristics of the PVA/PPy/GF hydrogel at different scan rates under ambient temperature are presented in Fig. 3(a). The absence of distinct redox peaks in all CV curves indicates the non-faradaic nature of the electrochemical process. The quasi-rectangular shape of the curves further suggests a dominant electrical double-layer capacitive behavior. To investigate the electrochemical response under thermal bias, a temperature difference of 5 K was applied across the hydrogel, and the corresponding CV measurements are shown in Fig. S6. The results confirm that no redox reactions are induced by the temperature gradient, and the observed current response originates solely from ion migration within the hydrogel matrix.

The thermal conductivity of PVA/PPy/UF and PVA/PPy/GF hydrogels with varying SDBS mass fractions was measured separately, as shown in Fig. 3(b). The thermal conductivity increases progressively with increasing SDBS loading, which can be attributed to the elevated ion concentration within the hydrogel matrix. Notably, however, the PVA/PPy/GF hydrogels demonstrate consistently lower thermal conductivity compared to the PVA/PPy/UF counterparts at equivalent mass fractions.

Electrochemical impedance spectroscopy was performed by applying an alternating voltage of $V_{ac}(f) = 10$ mV across the hydrogel-based capacitors. The resulting Nyquist plots for hydrogels with different SDBS mass fractions are presented in Fig. 3(c), from which the ionic conductivity is derived and summarized in Fig. 3(d). The results reveal a clear positive correlation between ionic conductivity and SDBS mass fraction, consistent with the increased charge carrier density. Importantly, the PVA/PPy/GF hydrogels exhibit approximately 10% lower ionic conductivity than the uniformly doped PVA/PPy/UF hydrogels across the concentration range of 2.50% to 7.50%. The differences in thermal and ionic conductivity can be attributed to the distinct spatial distribution of immobilized anions within the polymer matrix. In the uniformly doped system, SDBS anions are homogeneously immobilized throughout the hydrogel network, providing relatively uniform pathways for cation migration. This minimizes localized resistance and enables efficient ionic transport. In contrast, the gradient-doped PVA/PPy/GF hydrogels feature a concentration gradient of immobilized anions, with higher anion density near the hot side. This asymmetric distribution introduces spatial variations in local ion concentration and electrostatic potential, which can partially hinder cation migration due to localized charge accumulation and altered local electric fields. The PVA/PPy/GF hydrogel with a gradient-immobilized SDBS mass fraction of 5.00% exhibits a high ionic conductivity of 17.91 mS·cm^{-1} and a low thermal conductivity of 0.377 W·m^{-1}·K^{-1}, positioning it as a highly competitive material for ionic thermoelectric applications.

Analogous to electronic thermoelectric (e-TE) materials, the thermoelectric performance of i-TE materials can be evaluated by the dimensionless figure of merit (ZT), defined as:

$$ZT = \frac{\sigma S e^2 T}{\lambda} \tag{3}$$

where σ, λ, and T represent the ionic conductivity, thermal conductivity, and absolute temperature, respectively.

Notably, the optimized PVA/PPy/GF hydrogel achieves a maximum ZT value of 0.645, representing an approximately sixfold enhancement over the best-performing PVA/PPy/UF hydrogel. It should be noted that, unlike electronic thermoelectric materials, ionic thermoelectric devices operate in a capacitive mode. Therefore, the ZT value reported here

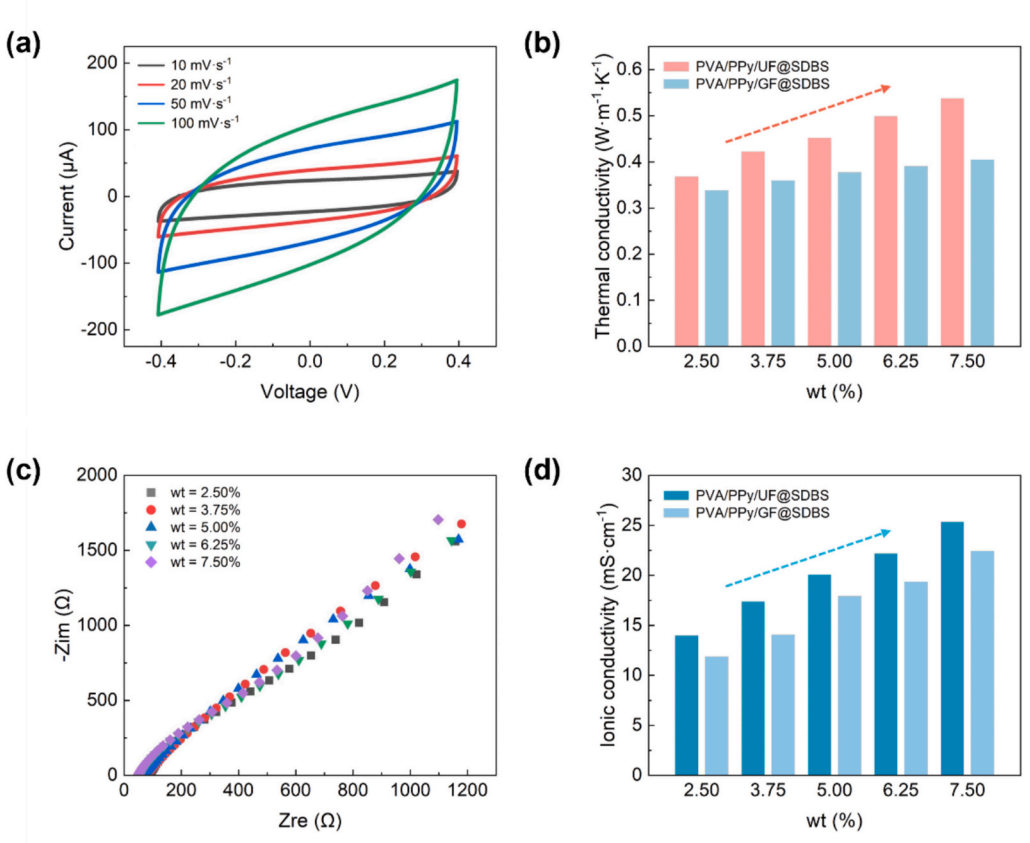

Fig. 3. Electrochemical performance, thermal and ionic transport properties of the hydrogels. (a) Cyclic voltammetry (CV) curves of the PVA/PPy/GF@5.00%SDBS hydrogel at different scan rates. (b) Thermal conductivity of PVA/PPy/UF and PVA/PPy/GF hydrogels as a function of SDBS mass fraction. (c) Nyquist plots of PVA/PPy/GF hydrogel with varying SDBS mass fractions. (d) Ionic conductivity of PVA/PPy/UF and PVA/PPy/GF hydrogels versus SDBS mass fraction.

serves as a material-level comparative parameter rather than a direct predictor of continuous power output.

3.4. Operating characteristics

Owing to the inability of ions to traverse external circuits, ionic thermoelectric generators operate in a capacitive energy conversion mode. The four working stages of ionic thermoelectric devices, along with the corresponding voltage variation process, are illustrated in Fig. 4(a) and 4(b). Initially, under an applied temperature gradient with an open external circuit, thermally driven ion migration leads to charge accumulation at the electrodes, resulting in a progressive rise in voltage (Stage I). Subsequently, when the external circuit is closed while the temperature gradient is maintained, the stored charges are discharged

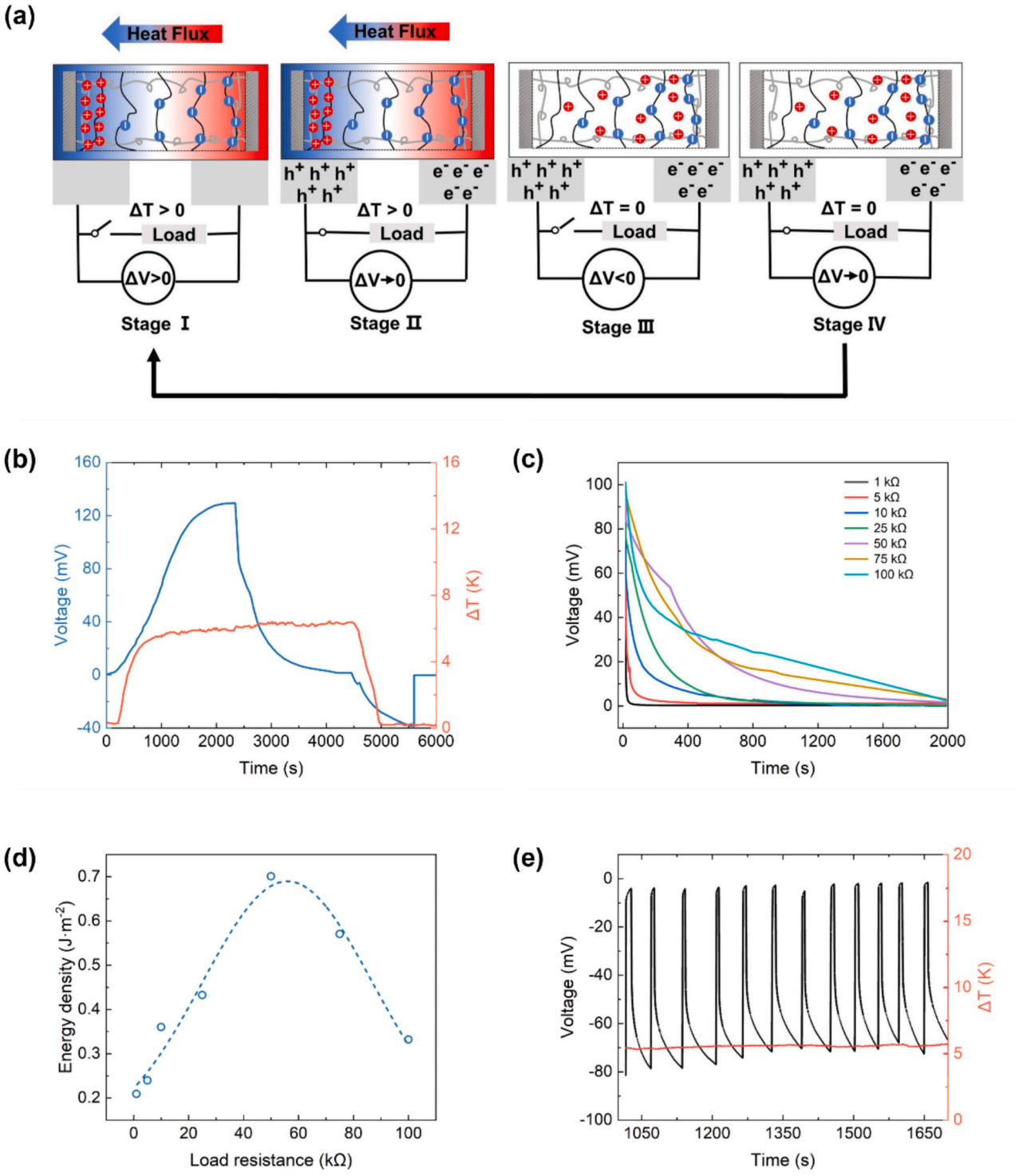

Fig. 4. Operational mechanism and performance of the i-TE supercapacitor. (a) Schematic diagram of the working mechanism in the four-stage i-TE supercapacitor cycle. (b) Voltage response of the PVA/PPy/GF@5.00%SDBS hydrogel under a 50 kΩ external load, illustrating the four operational stages. (c) Output voltage profiles and (d) energy densities measured during the discharge phase (Stage II) under different external loads at a temperature difference of ~5 K. (e) The charge/discharge voltage curve of cycle reliability test.

through the load, generating an electrical current and delivering work to the external circuit (Stage II). After the temperature gradient is removed and with the circuit still open, the ions gradually diffuse back toward their initial equilibrium distribution, causing the voltage to decay (Stage III). Finally, with the temperature gradient removed and the external circuit closed, any residual charge remaining on the electrodes flows through the load, returning the electrodes to their initial state and completing the cycle (Stage IV).

The PVA/PPy/GF@5.00%SDBS hydrogel was selected for capacitive performance evaluation due to its superior Seebeck coefficient among all investigated compositions. The hydrogel was positioned between two carbon electrodes (33 × 10 mm) with an inter-electrode spacing of 15 mm. A temperature difference of ~5 K was applied under ambient conditions to measure the induced thermovoltage. The output energy density was calculated using the following equation:

$$E = \int_0^t \left(\frac{V^2}{R}\right) dt \tag{4}$$

where V represents the voltage, R is the load resistance, and t is the discharge time. The calculated energy density ($J{\cdot}m^{-2}$) is normalized based on the effective electrode contact area.

Fig. 4(c) and (d) display the discharge profiles and corresponding energy density as a function of external load resistance. The energy density follows a parabolic trend, reaching a maximum value of 0.701 $J{\bullet}m^{-2}$ at an optimal load resistance of 50 kΩ. This substantial energy output under a minimal temperature gradient confirms the exceptional thermoelectric conversion capability of the developed hydrogel. The quasi-continuous operational characteristics were further investigated. As shown in Fig. 4(e), the device attained a saturation voltage of ~81 mV after 1000 s of charging under a ~ 4 K temperature difference. Subsequent connection to a 1 kΩ external load resulted in complete discharge to nearly 0 V within 5 s, followed by voltage recovery to the original level within 50 s. Remarkably, the material system maintained stable performance over 11 consecutive charge/discharge cycles within ~600 s, demonstrating excellent cycling stability.

4. Conclusions

In summary, this work demonstrates a substantial enhancement in thermoelectric performance through gradient immobilization of anions, supported by comprehensive theoretical and experimental analyses. By employing a novel strategy involving PPy-mediated immobilization of large anions, we have developed a series of high-performance ionic thermoelectric materials based on PVA hydrogels. The optimized PVA/PPy/GF hydrogel with gradient-anion immobilization achieves a remarkable Seebeck coefficient of 21.5 $mV{\cdot}K^{-1}$, representing 2.5-fold and 7-fold enhancements compared to uniformly immobilized and pristine systems, respectively. Furthermore, the hydrogel exhibits excellent ionic conductivity (17.91 $mS{\cdot}cm^{-1}$) coupled with low thermal conductivity (0.377 $W{\cdot}m^{-1}{\cdot}K^{-1}$), resulting in a significantly improved thermoelectric figure of merit (ZT = 0.645). The proposed gradient immobilization strategy offers a new paradigm for modulating ion transport pathways and enhancing thermoelectric performance in ionic conductive systems. With its cost-effective fabrication process, scalability, and outstanding thermoelectric properties, this hydrogel system presents a promising solution for efficient low-grade thermal energy harvesting.

CRediT authorship contribution statement

Zhou Li: Writing – original draft, Methodology, Data curation, Conceptualization. **Wenzhuo Zhao:** Writing – review & editing, Investigation, Conceptualization. **Shouze Li:** Methodology, Investigation, Formal analysis. **Dongyan Xu:** Supervision, Conceptualization. **Wonjoon Choi:** Supervision, Conceptualization. **Run Hu:** Supervision, Methodology, Funding acquisition, Conceptualization.

Declaration of competing interest

The authors declare that they have no known competing financial interests or personal relationships that could have appeared to influence the work reported in this paper.

Acknowledgements

The work is supported by the financial support from National Natural Science Foundation of China [NSFC No.52161160332].

Appendix A. Supplementary data

Supplementary data to this article can be found online at https://doi.org/10.1016/j.cej.2026.176570.

Data availability

Data will be made available on request.

References

[1] Y. He, Q. Zhang, H. Cheng, Y. Liu, Y. Shu, Y. Geng, Y. Zheng, B. Qin, Y. Zhou, S. Chen, J. Li, M. Li, G.O. Odunmbaku, C. Li, T. Shumilova, J. Ouyang, K. Sun, Role of ions in hydrogels with an ionic seebeck coefficient of 52.9 mV K^{-1}, J. Phys. Chem. Lett. 13 (2022) 4621–4627, https://doi.org/10.1021/acs.jpclett.2c00845.
[2] X. Shi, J. He, Thermopower and harvesting heat, Science 371 (2021) 343–344, https://doi.org/10.1126/science.abf3342.
[3] B. Yu, J. Duan, H. Cong, W. Xie, R. Liu, X. Zhuang, H. Wang, B. Qi, M. Xu, Z. L. Wang, J. Zhou, Thermosensitive crystallization–boosted liquid thermocells for low-grade heat harvesting, Science 370 (2020) 342–346, https://doi.org/10.1126/science.abd6749.
[4] W. Zhao, Z. Wang, R. Hu, X. Luo, Gel-based thermocells for low-grade heat harvesting, EPL Europhys. Lett. 135 (2021) 26001, https://doi.org/10.1209/0295-5075/ac2075.
[5] D. Zhao, H. Wang, Z.U. Khan, J.C. Chen, R. Gabrielsson, M.P. Jonsson, M. Berggren, X. Crispin, Ionic thermoelectric supercapacitors, Energy Environ. Sci. 9 (2016) 1450–1457, https://doi.org/10.1039/C6EE00121A.
[6] H. Sun, Y. Zhao, S. Jiao, C. Wang, Y. Jia, K. Dai, G. Zheng, C. Liu, P. Wan, C. Shen, Environment tolerant conductive nanocomposite organohydrogels as flexible strain sensors and power sources for sustainable electronics, Adv. Funct. Mater. 31 (2021) 2101696, https://doi.org/10.1002/adfm.202101696.
[7] P. Yang, K. Liu, Q. Chen, X. Mo, Y. Zhou, S. Li, G. Feng, J. Zhou, Wearable thermocells based on gel electrolytes for the utilization of body heat, Angew. Chem. Int. Ed. 55 (2016) 12050–12053, https://doi.org/10.1002/anie.201606314.
[8] A.R.M. Siddique, S. Mahmud, B.V. Heyst, A review of the state of the science on wearable thermoelectric power generators (TEGs) and their existing challenges, Renew. Sust. Energ. Rev. 73 (2017) 730–744, https://doi.org/10.1016/j.rser.2017.01.177.
[9] J. Wu, J.J. Black, L. Aldous, Thermoelectrochemistry using conventional and novel gelled electrolytes in heat-to-current thermocells, Electrochim. Acta 225 (2017) 482–492, https://doi.org/10.1016/j.electacta.2016.12.152.
[10] H. Zhou, T. Yamada, N. Kimizuka, Supramolecular thermo-electrochemical cells: enhanced thermoelectric performance by host–guest complexation and salt-induced crystallization, J. Am. Chem. Soc. 138 (2016) 10502–10507, https://doi.org/10.1021/jacs.6b04923.
[11] G. Wu, Y. Xue, L. Wang, X. Wang, G. Chen, Flexible gel-state thermoelectrochemical materials with excellent mechanical and thermoelectric performances based on incorporating Sn^{2+} /Sn^{4+} electrolyte into polymer/carbon nanotube composites, J. Mater. Chem. A 6 (2018) 3376–3380, https://doi.org/10.1039/C7TA11146K.
[12] L. Zhang, T. Kim, N. Li, T.J. Kang, J. Chen, J.M. Pringle, M. Zhang, A.H. Kazim, S. Fang, C. Haines, D. Al-Masri, B.A. Cola, J.M. Razal, J. Di, S. Beirne, D. R. MacFarlane, A. Gonzalez-Martin, S. Mathew, Y.H. Kim, G. Wallace, R. H. Baughman, High power density electrochemical thermocells for inexpensively harvesting low-grade thermal energy, Adv. Mater. 29 (2017) 1605652, https://doi.org/10.1002/adma.201605652.
[13] T. Li, X. Zhang, S.D. Lacey, R. Mi, X. Zhao, F. Jiang, J. Song, Z. Liu, G. Chen, J. Dai, Y. Yao, S. Das, R. Yang, R.M. Briber, L. Hu, Cellulose ionic conductors with high differential thermal voltage for low-grade heat harvesting, Nat. Mater. 18 (2019) 608–613, https://doi.org/10.1038/s41563-019-0315-6.
[14] B. Kim, J. Na, H. Lim, Y. Kim, J. Kim, E. Kim, Robust high thermoelectric harvesting under a self-humidifying bilayer of metal organic framework and hydrogel layer, Adv. Funct. Mater. 29 (2019) 1807549, https://doi.org/10.1002/adfm.201807549.

[15] C.-G. Han, X. Qian, Q. Li, B. Deng, Y. Zhu, Z. Han, W. Zhang, W. Wang, S.-P. Feng, G. Chen, W. Liu, Giant thermopower of ionic gelatin near room temperature, Science 368 (2020) 1091–1098, https://doi.org/10.1126/science.aaz5045.
[16] B. Kim, J.U. Hwang, E. Kim, Chloride transport in conductive polymer films for an n-type thermoelectric platform, Energy Environ. Sci. 13 (2020) 859–867, https://doi.org/10.1039/C9EE02399B.
[17] H. Cheng, X. He, Z. Fan, J. Ouyang, Flexible quasi-solid state ionogels with remarkable seebeck coefficient and high thermoelectric properties, Adv. Energy Mater. 9 (2019) 1901085, https://doi.org/10.1002/aenm.201901085.
[18] M. Jeong, J. Noh, M.Z. Islam, K. Kim, A. Sohn, W. Kim, C. Yu, Embedding aligned graphene oxides in polyelectrolytes to facilitate thermo-diffusion of protons for high ionic thermoelectric figure-of-merit, Adv. Funct. Mater. 31 (2021) 2011016, https://doi.org/10.1002/adfm.202011016.
[19] X. He, H. Cheng, S. Yue, J. Ouyang, Quasi-solid state nanoparticle/(ionic liquid) gels with significantly high ionic thermoelectric properties, J. Mater. Chem. A 8 (2020) 10813–10821, https://doi.org/10.1039/D0TA04100A.
[20] M. Frank, J. Pflaum, Tuning electronic and ionic transport by carbon-based additives in polymer electrolytes for thermoelectric applications, Adv. Funct. Mater. 32 (2022) 2203277, https://doi.org/10.1002/adfm.202203277.
[21] Z. Liu, H. Cheng, H. He, J. Li, J. Ouyang, Significant enhancement in the thermoelectric properties of ionogels through solid network engineering, Adv. Funct. Mater. 32 (2022) 2109772, https://doi.org/10.1002/adfm.202109772.
[22] Y. Li, Q. Li, X. Zhang, B. Deng, C. Han, W. Liu, 3D hierarchical electrodes boosting ultrahigh power output for gelatin-KCl-$FeCN^{4-/3-}$ ionic thermoelectric cells, Adv. Energy Mater. 12 (2022) 2103666, https://doi.org/10.1002/aenm.202103666.
[23] Z. Liu, H. Cheng, Q. Le, R. Chen, J. Li, J. Ouyang, Giant thermoelectric properties of ionogels with cationic doping, Adv. Energy Mater. 12 (2022) 2200858, https://doi.org/10.1002/aenm.202200858.
[24] Y. Zhou, Z. Dong, Y. He, W. Zhu, Y. Yuan, H. Zeng, C. Li, S. Chen, K. Sun, Multi-ionic hydrogel with outstanding heat-to-electrical performance for low-grade heat harvesting, Chem. Asian J. 17 (2022) e202200850, https://doi.org/10.1002/asia.202200850.
[25] Q. Chen, B. Chen, S. Xiao, J. Feng, J. Yang, Q. Yue, X. Zhang, T. Wang, Giant thermopower of hydrogen ion enhanced by a strong hydrogen bond system, ACS Appl. Mater. Interfaces 14 (2022) 19304–19314, https://doi.org/10.1021/acsami.1c24698.
[26] G. Fan, K. Liu, H. Su, Y. Luo, Y. Geng, L. Chen, B. Wang, Z. Mao, X. Sui, X. Feng, Mesoscopic confined ionic thermoelectric materials with excellent ionic conductivity for waste heat harvesting, Chem. Eng. J. 434 (2022) 134702, https://doi.org/10.1016/j.cej.2022.134702.
[27] S. Mardi, D. Zhao, N. Kim, I. Petsagkourakis, K. Tybrandt, A. Reale, X. Crispin, The interfacial effect on the open circuit voltage of ionic thermoelectric devices with conducting polymer electrodes, Adv. Electron. Mater. 7 (2021) 2100506, https://doi.org/10.1002/aelm.202100506.
[28] S. Mardi, D. Zhao, K. Tybrandt, A. Reale, X. Crispin, Interfacial effect boosts the performance of all-polymer ionic thermoelectric supercapacitors, Adv. Mater. Interfaces 9 (2022) 2201058, https://doi.org/10.1002/admi.202201058.
[29] J. Liu, W. Zeng, X. Tao, Gigantic effect due to phase transition on thermoelectric properties of ionic sol–gel materials, Adv. Funct. Mater. 32 (2022) 2208286, https://doi.org/10.1002/adfm.202208286.
[30] Y. Fang, H. Cheng, H. He, S. Wang, J. Li, S. Yue, L. Zhang, Z. Du, J. Ouyang, Stretchable and transparent ionogels with high thermoelectric properties, Adv. Funct. Mater. 30 (2020) 2004699, https://doi.org/10.1002/adfm.202004699.
[31] J. Xu, H. Wang, X. Du, X. Cheng, Z. Du, H. Wang, Highly stretchable PU ionogels with self-healing capability for a flexible thermoelectric generator, ACS Appl. Mater. Interfaces 13 (2021) 20427–20434, https://doi.org/10.1021/acsami.1c03328.
[32] Z.A. Akbar, J.-W. Jeon, S.-Y. Jang, Intrinsically self-healable, stretchable thermoelectric materials with a large ionic seebeck effect, Energy Environ. Sci. 13 (2020) 2915–2923, https://doi.org/10.1039/C9EE03861B.
[33] Z.A. Akbar, Y.T. Malik, D. Kim, S. Cho, S. Jang, J. Jeon, Self-healable and stretchable ionic-liquid-based thermoelectric composites with high ionic seebeck coefficient, Small 18 (2022) 2106937, https://doi.org/10.1002/smll.202106937.
[34] Y.T. Malik, Z.A. Akbar, J.Y. Seo, S. Cho, S. Jang, J. Jeon, Self-healable organic–inorganic hybrid thermoelectric materials with excellent ionic thermoelectric properties (adv. energy mater. 6/2022), Adv. Energy Mater. 12 (2022) 2270020, https://doi.org/10.1002/aenm.202270020.